magnetochemistry

MDPI

Article

Comparative Buffer and Spacer Layer Engineering in Co/Pt-Based Perpendicular Synthetic Antiferromagnets

Mehmet Emre Aköz [1,*], Frowin Dörr [2], Ahmet Yavuz Oral [3] and Yasser Shokr [4,5]

[1] Department of Nanoscience and Nanotechnology, Gebze Technical University, Kocaeli 41400, Türkiye
[2] Department of Physics, Freie Universitat, 14195 Berlin, Germany; f.doerr@fu-berlin.de
[3] Department of Material Science and Engineering, Gebze Technical University, Kocaeli 41400, Türkiye; aoral@gtu.edu.tr
[4] Nuclear Radiation Detectors Research and Development Center, Bolu Abant Izzet Baysal University, Bolu 14030, Türkiye; yashokr@gmail.com
[5] Faculty of Science, Department of Physics, Helwan University, Cairo 11795, Egypt
* Correspondence: akoz@gtu.edu.tr

Abstract

Perpendicular magnetic tunnel junctions (p-MTJs) rely on synthetic antiferromagnets (SAFs) as reference layers to achieve strong perpendicular magnetic anisotropy (PMA) together with stable interlayer exchange coupling. In this study, we present a comparative materials study of buffer and spacer layer engineering in Co/Pt-based perpendicular synthetic antiferromagnets (p-SAFs). The influence of buffer layer selection, number of multilayer repeats, and annealing at 330 °C for 30 min on PMA and interlayer exchange coupling is systematically examined. Co/Pt multilayers with four and six repeats were grown on Ta/Ru and Ta/CuN buffer layers separately, followed by the fabrication of SAF structures incorporating Ru spacers with thickness between 0.60 and 0.80 nm. Magnetic measurements show that Ta/Ru-buffered structures exhibit squarer hysteresis loops, higher remanence, and greater tolerance to annealing at 330 °C for 30 min compared to Ta/CuN-buffered counterparts. The SAF structures display clear two-step magnetization reversal and robust antiferromagnetic coupling across the investigated Ru thickness range, with large exchange fields and bias fields in the deposited state. Although annealing reduces the absolute coupling strength, a Ru spacer thickness of 0.60 nm retains the strongest antiferromagnetic response within the studied thermal budget. These results underscore the importance of comparative buffer and spacer layer engineering and provide materials insights into the design of Co/Pt-based p-SAF reference stacks that may inform future p-MTJ structures.

Keywords: buffer layer engineering; spacer layer engineering; perpendicular magnetic anisotropy; synthetic antiferromagnetic structures

Check for updates

Academic Editor: Fanny Béron

Received: 6 December 2025
Revised: 9 January 2026
Accepted: 13 January 2026
Published: 19 January 2026

Copyright: © 2026 by the authors. Licensee MDPI, Basel, Switzerland. This article is an open access article distributed under the terms and conditions of the Creative Commons Attribution (CC BY) license.

1. Introduction

Spintronics exploits both the charge and spin degrees of freedom of electrons to enable efficient information storage and manipulation at the nanoscale [1–4]. Among spintronic building blocks, magnetic tunnel junctions (MTJs) have attracted considerable attention owing to their non-volatility, fast operation, and low energy consumption, making them a central materials platform for modern spin-based technologies [1,2,5–17]. In particular, perpendicular magnetic tunnel junctions (p-MTJs) are preferred over in-plane configurations because their out-of-plane (OoP) magnetic orientation enables higher storage density and improved scaling behavior [4,18,19]. A central challenge in p-MTJ-related materials

systems is the realization of strong perpendicular magnetic anisotropy (PMA) in multilayer thin films, which is critically governed by interface quality and interlayer exchange coupling [18,20–23]. These factors directly influence the magnetic stability and scalability of the reference layer at reduced dimensions [19,22,24].

Synthetic antiferromagnets (SAFs) have therefore emerged as key materials components in p-MTJ architectures because they provide strong antiferromagnetic coupling while effectively suppressing stray fields acting on the free layer [19,22,25–27]. In a SAF structure, two ferromagnetic (FM) layers are separated by a non-magnetic (NM) spacer layer, giving rise to an indirect exchange interaction mediated by conduction electrons. This interaction, commonly described by the Ruderman–Kittel–Kasuya–Yosida (RKKY) interaction, oscillates in both sign and magnitude as a function of spacer thickness, enabling controlled access to antiferromagnetic coupling regimes [28–31]. Among commonly used spacer materials, Ru has been extensively employed due to its robust and reproducible interlayer exchange coupling, with a well-established antiferromagnetic maximum occurring at spacer thicknesses of approximately 0.60–0.80 nm in Co/Ru-based systems [32–34].

Recent studies have further advanced the understanding of interlayer exchange coupling, anisotropy control, and thermal effects in perpendicular SAF and MTJ-related multilayers [31,34,35]. These works demonstrate that spacer thickness, interfacial quality, and structural control play a critical role in stabilizing perpendicular magnetic orientation, while also highlighting the need for systematic material-based investigations that disentangle the respective roles of buffer layers and spacer layers.

Beyond spacer layer optimization, the buffer layer plays a decisive role in determining the microstructural quality and magnetic response of perpendicular multilayer structures. The buffer layer governs the initial growth conditions, influencing crystallographic texture, interface sharpness, and roughness propagation throughout the stack. These structural attributes, in turn, strongly affect the magnitude of PMA and the efficiency of interlayer exchange coupling in SAF structures [26,36–41]. Previous studies have shown that different buffer materials, such as Ru- and CuN-based buffers, can promote distinct growth modes and texturing in Pt/Co multilayers, leading to measurable differences in magnetic anisotropy and switching behavior.

Despite these insights, a systematic comparison of how buffer layer selection interacts with spacer layer thickness to shape the magnetic properties and annealing response of p-SAF multilayers remains limited. In particular, while the role of buffer layers in promoting initial growth is well-known, their specific influence on the thermal stability of RKKY-mediated interlayer exchange coupling remains poorly understood. In this study, we address this knowledge gap by systematically investigating the combined effects of buffer layer selection and Ru spacer thickness on the magnetic behavior of Co/Pt-based p-SAF structures.

Co/Pt multilayers with a varying number of repeats were grown on Ta/Ru and Ta/CuN buffer layers, followed by the fabrication of SAF stacks incorporating Ru spacers in the thickness range of 0.60–0.80 nm with 0.05 nm steps. This specific thickness window, corresponding to the most sensitive antiferromagnetic coupling regime of the RKKY interaction, was selected based on a previous study [42] and earlier systematic studies [43,44] that established the necessary foundation for narrowing the focus to this practically relevant regime. The magnetic properties were examined in the deposited state and after annealing at 330 °C for 30 min [45,46]. Rather than demonstrating device performance in a fully integrated junction, this study provides comparative, materials-based insights into how buffer and spacer layer engineering collectively govern the magnetic stability, reversal behavior, and annealing response of p-SAF reference stacks,

thereby offering structure–property-oriented guidance that may inform the design of future p-MTJ structures.

2. Experimental Setup

All thin films were fabricated under high-vacuum (HV) conditions with a base pressure of approximately 1×10^{-7} mbar. Each layer was deposited at room temperature by e-beam evaporation onto Si (100) substrates. Prior to deposition, the substrates were cleaned sequentially in ultrasonic baths of distilled water, ethanol, and isopropanol for 10 min each to ensure a contaminant-free surface. The thickness of all layers was controlled using quartz crystal microbalance (QCM) monitoring to ensure reproducible deposition rates. The QCM calibration was cross-checked by X-ray photoelectron spectroscopy (XPS) to establish reliable relative thickness control between different deposition runs. While this approach does not claim monolayer deviation absolute accuracy, it provides sufficient precision for comparative and trend-based analysis [47–50], which is the primary focus of this study. After deposition, part of the sample set was annealed at 330 °C for 30 min, while the remaining samples were kept in the deposited state to evaluate the effect of thermal treatment.

The influence of the buffer layer on the perpendicular magnetic anisotropy (PMA) of Co/Pt multilayers was investigated using VSM measurements in both deposited and annealed conditions. Two series of samples were prepared with different buffer configurations: $[Ta/CuN]_3$ and $[Ta/Ru]_3$. For each buffer type, Co/Pt multilayers were fabricated by repeating the bilayer sequence [Co (0.35 nm)/Pt (0.15 nm)] four or six times. Out-of-plane hysteresis loops were recorded before and after annealing to evaluate the effect of buffer configuration on PMA and the thermal stability of the multilayers.

Subsequently, five additional synthetic antiferromagnetic (SAF) samples were prepared with different Ru spacer thickness of x = 0.60, 0.65, 0.70, 0.75, and 0.80 nm. Each SAF structure included a central Ru spacer inserted between two Co layers (each layer with a thickness of 0.35 nm) to enable antiferromagnetic coupling [33,37,51]. The SAF core was embedded between two asymmetric Co/Pt multilayer stacks, six repetitions below and four repetitions above the spacer. The complete multilayer configuration was: $[Co\ (0.35\ nm)/Pt\ (0.15\ nm)]_6/Co\ (0.35\ nm)/Ru\ (z)/Co\ (0.35\ nm)/[Pt\ (0.15\ nm)/Co\ (0.35\ nm)]_4$, where z denotes the Ru spacer thickness. The architectural details of these stacks are illustrated in Figure 1a,b, which provide a schematic representation of the buffer layer variations and the complete SAF multilayer sequence, respectively. These diagrams highlight the asymmetric arrangement of the Co/Pt repeats (six below and four above the Ru spacer) to facilitate layer-resolved switching analysis. As in the buffer layer series, half of the SAF samples were annealed at 330 °C for 30 min, while the remaining samples were analyzed in the deposited condition. Magnetic characterization under both conditions was performed using Vibrating sample magnetometer (VSM) by measuring the OoP hysteresis loops to determine interlayer coupling behavior and thermal stability.

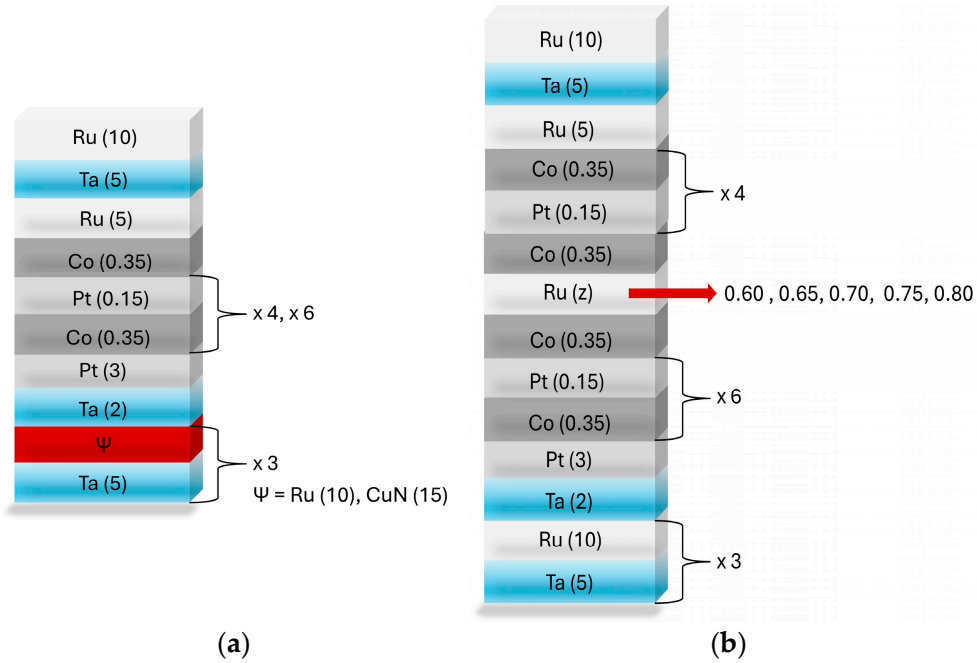


Figure 1. Schematic illustration of the sample structure used in this study: (**a**) Co/Pt multilayers with different buffer layers (Ta/CuN and Ta/Ru) and bilayer repetitions used to investigate the effect of the buffer layer on PMA; (**b**) SAF structures with a central Ru spacer between two Co layers, embedded between asymmetric Co/Pt stacks. The numbers in parentheses indicate the layer thickness in nanometers (nm).

3. Results

Figure 2a–d show the out-of-plane VSM loops of the Co/Pt multilayers on Ta/Ru and Ta/CuN buffers. In Figure 2a, the deposited loop is rounded with low coercivity and reduced remanent magnetization, indicating a broad distribution of switching fields and limited perpendicular magnetic anisotropy (PMA). After annealing, although the remanence increased and the transition became slightly steeper, the gradual approach to saturation persisted, suggesting that the PMA remained limited in this configuration. In contrast, the Ta/Ru buffer (Figure 2c,d) provides sharp switching and higher squareness even in deposited state. Annealing further sharpens these transitions and reduces the high-field tail, which is consistent with improved interfacial quality.

The panel-by-panel comparison reveals that increasing the number of repeats from 4 to 6 strengthens PMA for both buffers. However, at a fixed number of repeats, the Ta/Ru buffer demonstrates superior squareness and better retention of magnetic properties after thermal treatment. These behaviors are consistent with the known ability of Ru buffers to promote favorable growth texture in Co/Pt multilayers, thereby enhancing annealing tolerance compared to CuN-based structures. No exchange-bias-like shift in the loop center was observed across any of the samples [52,53].

For the Ta/Ru buffer (Table 1), the deposited H_C is high and nearly independent of the number of repeats, remaining at approximately 943 Oe for both number of repeats (NoR) = 4 and 6. This stability is consistent with the square hysteresis loops observed in Figure 2c,d. Annealing at 330 °C for 30 min raised H_C uniformly to 1041–1050 Oe range, representing a relative increase of approximately 10–11%. The weak positive slope of H_C with respect to NoR after annealing suggests that adding repeats slightly reinforces pinning and effective anisotropy. However, the dominant factor is the Ru-based buffer, which already promotes strong PMA even in the thinner stacks. Furthermore, the absence of

a loop offset and similar before and after annealing values indicate that Ru buffer sustains the interfacial order under thermal load with minimal degradation.

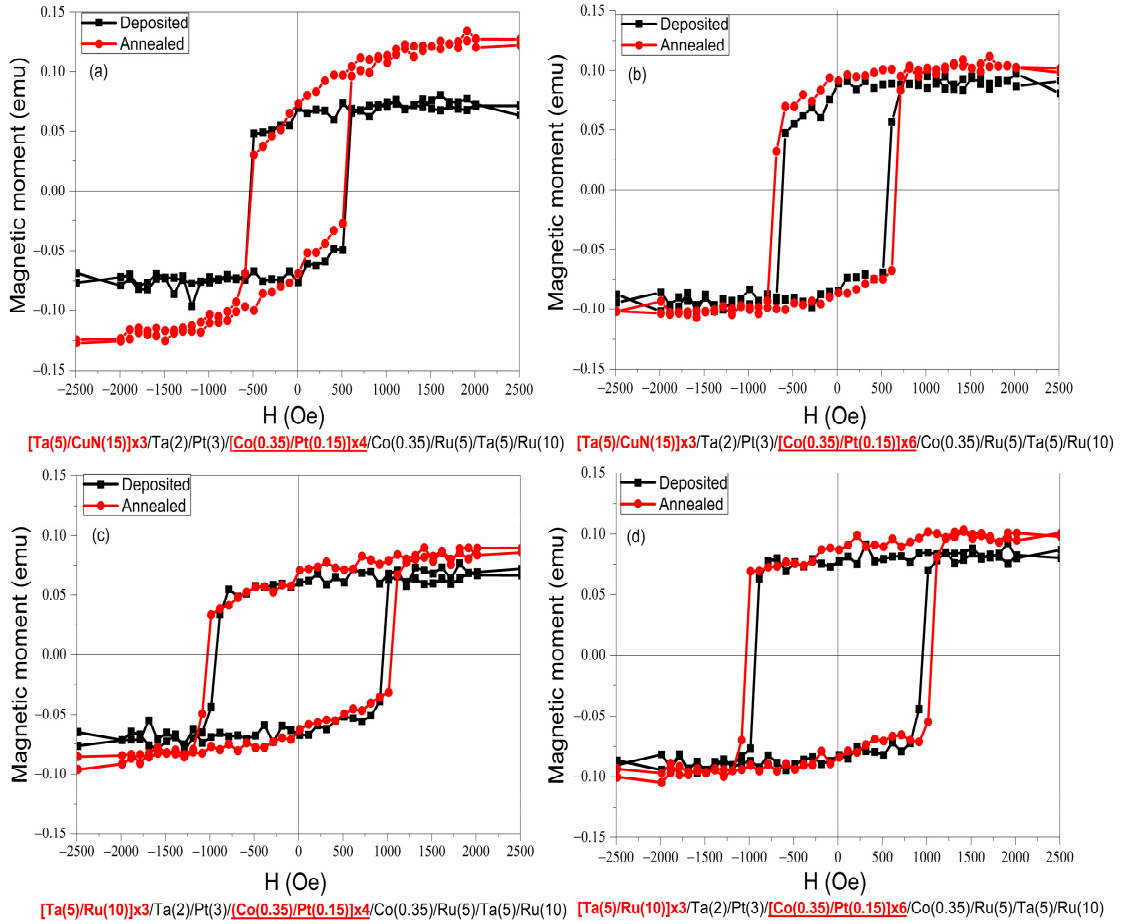


Figure 2. Out-of-plane hysteresis loops at room temperature for Co/Pt multilayers grown on two buffer structures and with two repetition numbers. Panel assignments: (**a**) Ta/CuN buffer, [Co (0.35)/Pt (0.15)]x4; (**b**) Ta/CuN buffer, [Co (0.35)/Pt (0.15)]x6; (**c**) Ta/Ru buffer, [Co (0.35)/Pt (0.15)]x4; (**d**) Ta/Ru buffer, [Co (0.35)/Pt (0.15)]x6. Layer thickness is given in parentheses in nanometers (nm). The black and red curves represent the deposited and annealed samples, respectively, the latter having been annealed at 330 °C for 30 min.

Table 1. Coercive field H_C versus number of repeats of Co/Pt (NoR = 4, 6) for multilayers grown on Ta/Ru and Ta/CuN buffers, measured before and after annealing at 330 °C for 30 min (Buffer Layer/Ta(2)/Pt(3)/[Co(0.35)/Pt(0.15)]xNoR/Co(0.35)/Ru(5)/Ta(5)/Ru(10).

Buffer Layer	NoR	Before Annealing	After Annealing at 330 °C
[Ta(5)/Ru(10)]x3	4	943 Oe	1041 Oe
	6	943 Oe	1050 Oe
[Ta(5)/CuN(15)]x3	4	540 Oe	528 Oe
	6	595 Oe	924 Oe

For the Ta/CuN buffer (Table 1), the deposited H_C was significantly lower than the Ru-buffered samples and showed a dependence on the number of repeats, increasing from 540 Oe at NoR = 4 to 595 Oe at NoR = 6. Annealing produced a contrasting response: for NoR = 4, H_C slightly decreases to ~528 Oe (reduction of approximately −2%), which is consistent with the rounded loop and persistent high-field tail in Figure 2a. This degradation points

to intermixing or roughening at the Ta/CuN interfaces, which weakens PMA in the thinner stacks. In contrast, for NoR = 6, H_C increased markedly to approximately 924 Oe (an enhancement of +55%). This indicates that the thicker Co/Pt stacks partly compensate for the adverse effect of CuN buffer during annealing, likely by stabilizing the growth texture and reducing the local dispersion of the switching fields. Despite this improvement, the best-performing CuN-based sample after annealing remains below the performance of Ru-buffered samples with fewer repeats (943 Oe < 1041 Oe), underscoring that the buffer structure, rather than number of repeats alone, governs the annealing tolerance at 330 °C and achievable coercivity.

All perpendicular SAFs with Ru spacers of 0.60–0.80 nm exhibited a two-step reversal on both branches of the hysteresis loop. On the descending branch (field reduced from $^{+}$H to $^{-}$H), the first step at H_{RD} (High-to-Right Decreasing) corresponds to the switching upper (thinner) Co/Pt stack, followed by the second step at H_{LD} (High-to-Low Decreasing) for the lower (thicker) stack. The ascending branch ($^{-}$H → $^{+}$H) symmetrically shows the switching of the upper and lower stacks at H_{LU} (High-to-Low Increasing) and H_{RU} (High-to-Right Increasing), respectively. For a representative sample with Ru = 0.80 nm, the descending loop steps occurred near +1794 Oe (upper layer) and −1583 Oe (lower layer). The central antiparallel (AP) plateau was essentially flat in the deposited state. After annealing at 330 °C for 30 min, the two-step structure was retained. However, AP plateau developed a slight positive slope, and the step fields shifted toward the origin. The step fields shifted toward the origin, as seen most clearly for Ru = 0.80 nm spacer in Figure 3.

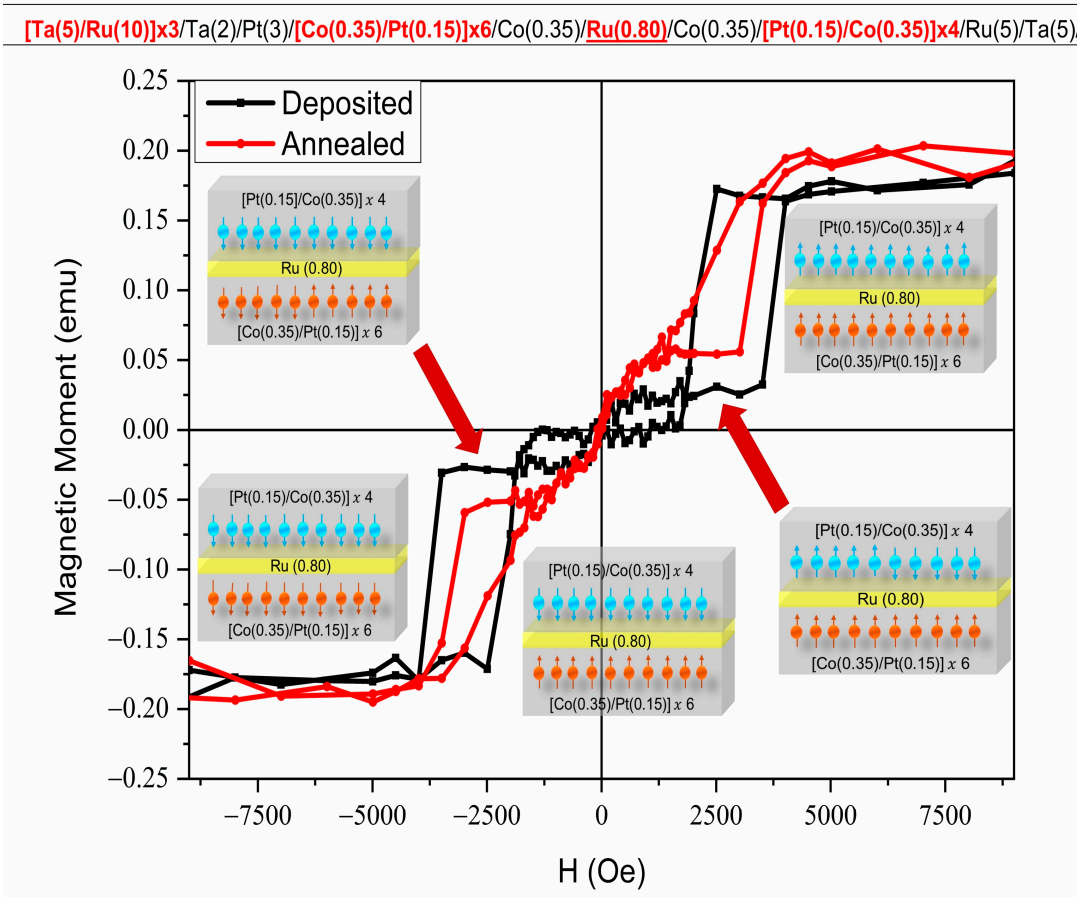


Figure 3. Perpendicular SAF hysteresis loop for Ru = 0.80 nm measured in the deposited state and after annealing at 330 °C for 30 min. The blue and red spheres represent the magnetization orientation of the upper and lower buffer–spacer Co/Pt stacks, respectively. Layer thickness is given in parentheses in nanometers (nm).

Figure 4 presents the exchange fields magnitudes calculated as $H_{ex}^{U} = (H_{RD} - H_{RU})/2$ for the upper stack and $H_{ex}^{L} = (H_{LD} - H_{LU})/2$ for the lower stack. In the deposited state, both $|H_{ex}^{U}|$ and $|H_{ex}^{L}|$ fall in the ~2045–2904 Oe range for Ru thickness of 0.60–0.80 nm, exhibiting a relatively weak thickness dependence. After annealing, $|H_{ex}|$ decreases for all spacer thickness; with the most significant fractional reductions occurring in the 0.70–0.80 nm range. while the 0.60 nm spacer retains the highest $|H_{ex}|$ among the annealed set, indicating superior robustness at this thickness.

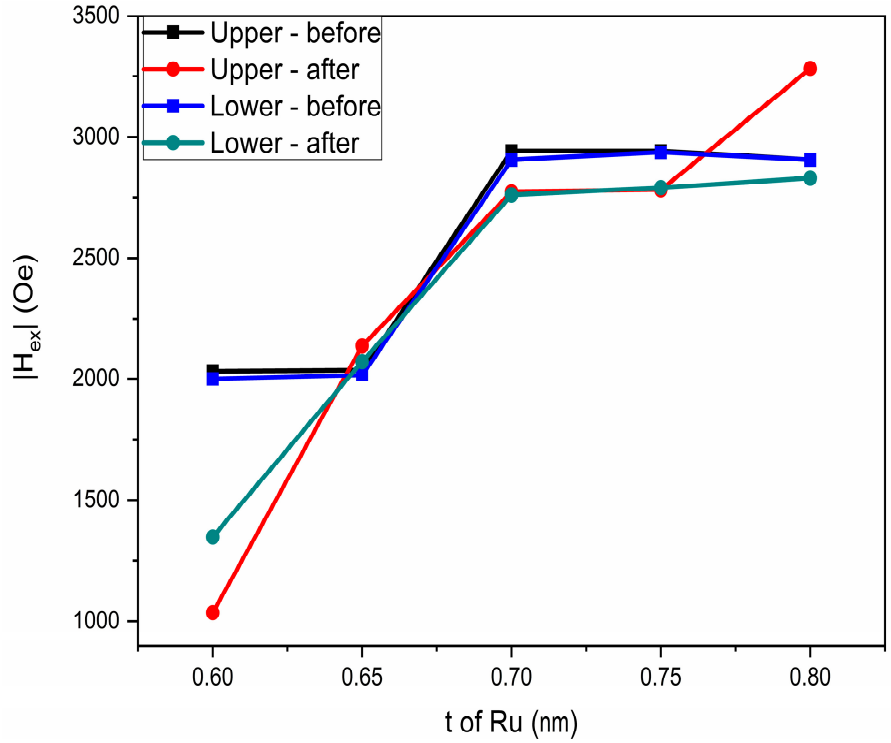


Figure 4. Exchange field magnitude $|H_{ex}|$ of the upper (multilayer between spacer layer and cap layer) and lower (multilayer between buffer layer and spacer layer) Co/Pt stacks as a function of Ru spacer thickness. Data for deposited and annealed (330 °C, 30 min) samples are shown on the same axis.

The variation of $|H_{ex}|$ as a function of Ru spacer thickness reveals a clear transition toward a strongly antiferromagnetically coupled regime. At Ru ≈ 0.60–0.65 nm, $|H_{ex}|$ remains moderate, suggesting that the coupling is still evolving toward its peak antiferromagnetic phase, which is more fully realized as the thickness approaches 0.70–0.80 nm. As the Ru spacer thickness reaches ~0.80 nm, a marked increase in $|H_{ex}|$ to nearly 2900 Oe is observed across all conditions, signifying the onset of strong RKKY coupling. While the absolute magnitude of $|H_{ex}|$ generally decreases after annealing, the Ru-thickness dependence becomes significantly clearer, suggesting that thermal treatment reduces sample-to-sample dispersion and improves thickness selectivity. In particular, the upper stack at 0.80 nm shows improved coupling efficiency relative to the other annealed samples, likely due to interdiffusion-enabled structural relaxation and interfacial sharpening. Collectively, these trends demonstrate that Ru spacer thickness and annealing treatment are decisive in tuning the magnitude and symmetry of exchange interactions, with the most balanced and stable coupling emerging near 0.80 nm.

Figure 5 shows the bias fields versus Ru thickness. Bias fields were calculated as $\mathbf{H_{bias}^{U}} = (H_{RD} + H_{RU})/2$ for upper stack and $\mathbf{H_{bias}^{L}} = (H_{LD} + H_{LU})/2$ for lower stack. The consistently large bias field magnitude (≈±800 Oe) observed across all SAF structures reflects the strong exchange mediated pinning and systematic loop-step offset inherent

to the SAF structure. Such persistent biasing demonstrates that AP alignment remains energetically favored even under thermal perturbation, underscoring the high thermal tolerance of the reference layers. This behavior is relevant at the materials level because a well-stabilized reference magnetization suppresses stray-field effects and enables more predictable device operation. The opposite bias field polarities measured for the upper and lower stacks confirm the balanced yet counteracting exchange fields required to sustain synthetic antiferromagnetic alignment. After annealing, the upper stack shows a reduction in $|H_{bias}|$, particularly at larger Ru thicknesses (e.g., 0.80 nm), suggesting that thermal processing partially relaxes the pinning conditions, potentially through modifications in exchange interaction strength or interfacial roughness. In contrast, the lower stack shows consistently negative $|H_{bias}|$ values with smaller magnitudes, signifying opposite direction biasing. Annealing slightly increases $|H_{bias}|$ for the lower stack, implying improved coupling uniformity and reduced asymmetry between the two magnetic stacks. Overall, the data demonstrate that while Ru thickness modulates the biasing behavior modestly, annealing plays a more significant role in rebalancing the exchange bias between the stacks.

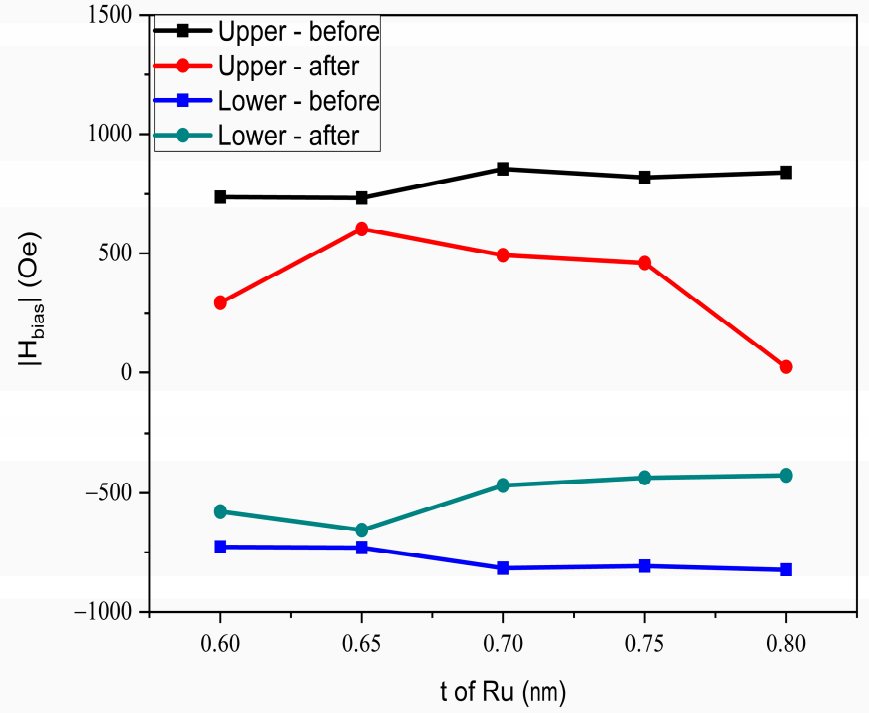


Figure 5. H_{bias} for the upper and lower stacks vs. Ru thickness; signed values are indicated. Before results shown as deposited and after results shown as annealed (330 °C, 30 min) samples on the same axis. Also, upper results shown as multilayer between spacer layer and cap layer (Blue atoms in Figure 3); and lower results shown as multilayer between buffer layer and spacer layer (Red atoms in Figure 3) Co/Pt stacks.

Using M_s(Co) ≈ 1.4 MA/m and total Co thickness of 1.75 nm (upper stack) and 2.45 nm (lower stack), the interlayer exchange coupling energy density J was estimated from $J \approx \mu_0 \cdot M_s \cdot t_{stack} \cdot |H_{ex}|$ values were obtained from independently measured out-of-plane hysteresis loops of corresponding Pt/Co multilayers, representing the effective magnetization including interfacial contributions. While alternative definitions of J exist in established studies, a single consistent definition is applied here to evaluate comparative coupling trends.

The J profile displays a distinct thickness-dependent behavior characterized by a shallow minimum near a Ru thickness of 0.75 nm. This localized reduction is inter-

preted as a transition region within the oscillatory cycle, where the constructive interference of spin-polarized electron waves is partially diminished due to a deviation from the optimal RKKY interaction. The sharpening of the J coupling profile and the clearer definition of this minimum after thermal treatment are consistent with thermally induced interface reconstruction.

By reducing interfacial disorder, annealing allows the intrinsic periodic nature of the RKKY interaction to emerge more prominently, even as the absolute coupling magnitude may decrease due to subtle interdiffusion. This sharpening, despite the reduction in magnitude, is attributed to thermal activation providing sufficient energy for atomic rearrangement and structural relaxation at the Co/Ru interfaces. This process refines the efficiency of the RKKY-mediated exchange pathways within specific thickness range. While excessive thermal budgets typically degrade coupling through intermixing, our results suggest that 330 °C annealing stays within the regime where atomic ordering dominates over roughness propagation, ultimately stabilizing the overall coupling behavior.

Collectively, the analysis of Figures 4–6 demonstrates that Ru spacer thickness and after annealing treatment play decisive roles in tuning the magnetic coupling characteristics of p-SAF structures. While deposited samples exhibit relatively moderate and thickness insensitive exchange coupling and bias fields, whereas annealing at 330 °C refines the thickness-dependent sensitivity of the exchange interaction, particularly near the optimal RKKY coupling regions. Simultaneously, annealing redistributes the bias fields between the upper and lower stacks, partially reducing the upper layer pinning while improving uniformity in the lower stacks. Overall, the results indicate that thermal activation stabilizes the magnetic configuration and promotes more balanced biasing across the multilayer stack. This refinement of the coupling profile and the stabilization of the antiparallel state are crucial for the development of high-performance p-MTJ devices, as they ensure robust reference layer pinning and predictable switching behavior under thermal load [38,51,54].

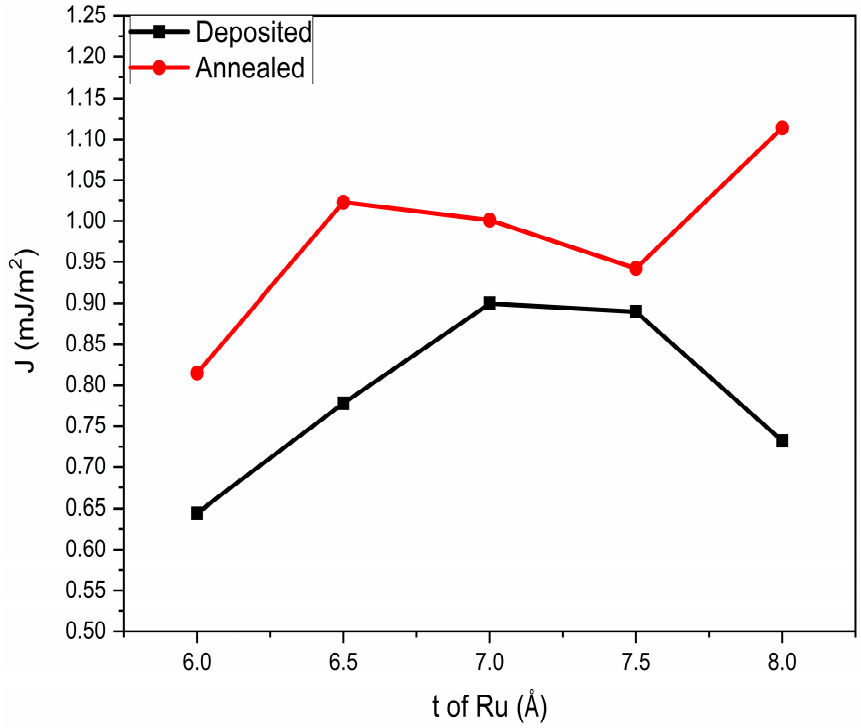


Figure 6. Interlayer exchange coupling energy density J as a function of Ru spacer thickness for deposited and annealed (330 °C, 30 min) SAF samples.

4. Discussion and Conclusions

This study aims to investigate systematic and comparative magnetic trends associated with buffer layer selection and Ru spacer thickness, rather than to extract statistically averaged absolute magnetic parameters. Accordingly, all samples were prepared under identical deposition and annealing conditions, and the results are interpreted as relative, trend-oriented indicators. Possible sample-to-sample variability in ultra-thin magnetic structures is acknowledged, while a comprehensive statistical analysis is within the scope of future studies.

All Co/Pt multilayers grown on Ta/Ru showed squarer loops, higher remanence, and larger coercivity than those on Ta/CuN at the same number of repeats. This behavior is consistent with the buffer-layer-controlled texture: Ru (and Pt) seeds favor a strong face-centered cubic (FCC) (111) template that promotes sharp Co/Pt interfaces and robust PMA, whereas amorphous poorly textured seeds (e.g., Ta or CuN) tend to degrade the perpendicular anisotropy. In Co-based multilayers, Ru and Pt underlayers have been well documented to transmit the (111) texture and stabilize PMA, even at small total thickness [30,32,40,55]. Upon annealing, the Ru-seeded films retained rectangular switching with only modest shifts in the step fields, whereas the CuN-seeded films showed weaker improvements and broader transitions. The observed small reduction in the PMA and increased rounding after thermal treatment are compatible with interfacial intermixing/roughening at the Co/Pt interfaces (particularly the top Co/Pt), which diminishes surface anisotropy and sharpness. This trend has been widely reported for Pt/Co stacks and related trilayers after annealing [33,41]. All the above support the recommendation that we start using Ru to make the SAF multilayer.

For the perpendicular SAFs with Ru spacers of 0.6–0.80 nm, all exhibited a clean two-step reversal on both branches, with the upper (thinner) Co/Pt stack switching first, producing an antiparallel magnetization plateau, followed by the switching of the lower (thicker) stack back to the parallel state. This steplike loop shape and layer-resolved switching are hallmark signatures of synthetic antiferromagnets, consistent with RKKY-mediated antiferromagnetic coupling across sub-nanometer Ru spacers. The thickness window we explored (approximately 0.60–0.80 nm) coincides with the strong AF-coupling region of the Co/Ru systems reported in classic interlayer exchange coupling studies and modern perpendicular SAFs [30,32,34,35,54].

The step fields were analyzed as explained previously for all samples. This step-based extraction is standard in the SAF loop analysis and directly reflects layer-resolved reversal fields. In our thickness series, deposited $|H_{ex}|$ clustered around ~2045–2904 Oe for both stacks at Ru = 0.60–0.80 nm with weak thickness dependence; after annealing at 330 °C for 30 min, $|H_{ex}|$ decreased for all spacers, most strongly at 0.70–0.80 nm, while 0.60 nm retained the largest $|H_{ex}|$. Meanwhile, the bias fields remained large ($\approx \pm 800$ Oe) and nearly thickness-independent before and after annealing, indicating that the loop centers for each stack remained well-defined despite the reduced step separation. These trends follow the known sensitivity of the Co/Ru RKKY coupling to spacer thickness and thermal budget [22,24,30].

For an energy scale comparison, we estimated the interlayer exchange energy density using the step-field method widely employed for SAFs, $J \approx M_s \cdot t_{stack} \cdot |H_{ex}|$, noting that different conventions can introduce a factor of two depending on the symmetry and unit system. With $M_s(Co) \approx 1.4$ MA/m and the total Co thickness of the upper/lower stacks from our design, J peaks near Ru at 0.80 nm in the deposited state and drops uniformly after annealing, with the 0.80 nm spacer retaining the largest annealing J. This thickness trend and the anneal-induced reduction are consistent with prior interlayer exchange coupling studies of Co/Ru and with recent perpendicular SAF reports [31,33,54].

The main conclusions derived from this dataset are as follows: (i) Ru-seeded Co/Pt stacks deliver superior PMA and improved magnetic robustness against annealing at 330 °C for 30 min compared to CuN-seeded stacks at the same number of repeats. This enhancement is highly consistent with the establishment of a strong (111) texture and superior interface quality, as widely documented in prior studies for Ru seed layers. (ii) All Ru-spacer SAFs (0.60–0.80 nm) show robust two-step switching with a flat AP plateau deposited and a slight positive plateau slope after annealing. (iii) Annealing at 330 °C for 30 min reduces $|H_{ex}|$ and the derived J across the thickness series, mostly at 0.70–0.80 nm, whereas bias fields remain large. (iv) Within the annealed set, Ru = 0.60 nm retains the strongest coupling. These findings align with the established Ru-mediated RKKY interaction and the reports on seed-layer-controlled PMA and interfacial thermal effects in Pt/Co systems [30–34,40,41,54,55].

Author Contributions: Conceptualization, M.E.A. and Y.S.; methodology, M.E.A., A.Y.O. and Y.S.; software, M.E.A. and Y.S.; validation, M.E.A. and Y.S.; formal analysis, M.E.A. and Y.S.; investigation, M.E.A. and F.D.; resources, M.E.A., F.D. and Y.S.; data curation, M.E.A. and Y.S.; writing—original draft preparation, M.E.A.; writing—review and editing, F.D., A.Y.O. and Y.S.; visualization, M.E.A.; supervision, A.Y.O. and Y.S.; project administration, M.E.A.; funding acquisition, M.E.A. and Y.S. All authors have read and agreed to the published version of the manuscript.

Funding: This research was funded by TUBITAK, grant number 124C509.

Data Availability Statement: The data presented in this study are available from the corresponding author upon reasonable request.

Conflicts of Interest: The authors declare no conflicts of interest.

References

1. Thomas, L.; Jan, G.; Zhu, J.; Liu, H.; Lee, Y.J.; Le, S.; Tong, R.Y.; Pi, K.; Wang, Y.J.; Shen, D.; et al. Spin-transfer torque devices for magnetic random access memory. *J. Appl. Phys.* **2014**, *115*, 172615.
2. Cai, H.; Kang, W.; Wang, Y.; De Barros Naviner, L.A.; Yang, J.; Zhao, W. High performance MRAM with spin-transfer-torque and voltage-controlled magnetic anisotropy effects. *Appl. Sci.* **2017**, *7*, 929.
3. Endoh, T.; Honjo, H. A recent progress of spintronics devices for integrated circuit applications. *J. Low Power Electron. Appl.* **2018**, *8*, 44. [CrossRef]
4. Bhatti, S.; Sbiaa, R.; Hirohata, A.; Ohno, H.; Fukami, S.; Piramanayagam, S.N. Spintronics based random access memory: A review. *Mater. Today* **2017**, *20*, 530–548. [CrossRef]
5. Maciel, N.; Marques, E.; Navier, L.; Zhou, Y.; Cai, H. Magnetic Tunnel Junction Applications. *Sensors* **2020**, *20*, 121.
6. Krizakova, V.; Perumkunnil, M.; Couet, S.; Gambardella, P.; Garello, K. Spin-orbit torque switching of magnetic tunnel junctions for memory applications. *J. Magn. Magn. Mater.* **2022**, *562*, 169692. [CrossRef]
7. Peng, S.; Zhu, D.; Li, W.; Wu, H.; Grutter, A.J.; Gilbert, D.A.; Lu, J.; Xiong, D.; Cai, W.; Shafer, P.; et al. Exchange Bias Switching in an Antiferromagnet/Ferromagnet Bilayer Driven by Spin–Orbit Torque. *Nat. Electron.* **2020**, *3*, 757–764.
8. Jungwirth, T.; Marti, X.; Wadley, P.; Wunderlich, J. Antiferromagnetic Spintronics. *Nat. Nanotechnol.* **2016**, *11*, 231–241. [CrossRef]
9. Wadley, P.; Howells, B.; Zelezny, J.; Andrews, C.; Hills, V.; Campions, R.P.; Novak, V.; Olejnik, K.; Maccheerozzi, F.; Dhesi, S.S.; et al. Electrical Switching of an Antiferromagnet. *Science* **2016**, *351*, 587–590. [CrossRef] [PubMed]
10. Lau, Y.C.; Betto, D.; Rode, K.; Coey, J.M.D.; Stamenov, P. Spin–Orbit Torque Switching without An External Field Using Interlayer Exchange Coupling. *Nat. Nanotechnol.* **2016**, *11*, 758–762. [CrossRef]
11. van der Brink, A.; Vermijs, G.; Solignac, A.; Koo, J.; Kohlhepp, J.T.; Swagten, H.J.M.; Koopmans, B. Field-Free Magnetization Reversal by Spin-Hall Effect and Exchange Bias. *Nat. Commun.* **2016**, *7*, 10854. [CrossRef]
12. Huang, D.; Lattery, D.; Liu, J.; Wang, X. Materials Engineering Enabled by Time-Resolved Magneto-Optical Kerr Effect for Spintronic Applications. *ACS Appl. Electron. Mater.* **2020**, *3*, 119–127. [CrossRef]
13. Sharma, B.; Bhutia, P.R.; Raj, R.K.; Chettri, B.; Kaushik, B.K.; Shreya, S. VCMA Gradient-Driven Skyrmion on a Trapezoidal Nanotrack for Racetrack Memory Application. *IEEE Open J. Nanotechnol.* **2025**, *6*, 44–50. [CrossRef]
14. Thapa, A.; Chettri, B.; Pradhan, P.C.; Sharma, B. First-principle Study of CrO_2-BNNT-CrO_2 Based MTJ Device Using EHTB Model and Its Application in a MRAM Circuit. *Mater. Today Commun.* **2024**, *39*, 108841. [CrossRef]

15. Razavi, S.A.; Wu, D.; Yu, G.; Lau, Y.-C.; Wong, K.L.; Zhu, W.; He, C.; Zhang, Z.; Coey, J.M.D.; Stamenov, P.; et al. Joule Heating Effect on Field-Free Magnetization Switching by Spin-Orbit Torque in Exchange-Biased Systems. *Phys. Rev. Appl.* **2017**, *7*, 024023. [CrossRef]
16. Kimata, M.; Chen, H.; Kondou, K.; Sugimoto, S.; Muduli, P.K.; Ikhlas, M.; Omori, Y.; Tomita, T.; MacDonald, A.H.; Nakatsuji, S.; et al. Magnetic and magnetic inverse spin Hall effects in a non-collinear antiferromagnet. *Nature* **2019**, *565*, 627–630. [CrossRef] [PubMed]
17. Lin, P.-H.; Yang, B.-Y.; Tsai, M.-H.; Chen, P.-C.; Huang, K.-F.; Lin, H.-H.; Lai, C.-H. Manipulating exchange bias by spin–orbit torque. *Nat. Mater.* **2019**, *18*, 335–341. [CrossRef]
18. Ikeda, S.; Miura, K.; Yamamoto, H.; Mizunuma, K.; Gan, H.D.; Endo, M.; Kanai, S.; Hayakawa, J.; Matsukura, F.; Ohno, H. A perpendicular-anisotropy CoFeB–MgO magnetic tunnel junction. *Nat. Mater.* **2010**, *9*, 721–724. [CrossRef]
19. Khanal, P.; Zhou, B.; Andrade, M.; Dang, Y.; Davydov, A.; Habiboglu, A.; Saidian, J.; Laurie, A.; Wang, J.P.; Gopman, D.B.; et al. Perpendicular magnetic tunnel junctions with multi-interface free layer. *Appl. Phys. Lett.* **2022**, *563*, 169914. [CrossRef]
20. Palin, V.; Guillemard, C.; de Melo, C.; Migot, S.; Gargiani, P.; Valvidares, M.; Bertran, F.; Andrieu, S. Engineering of perpendicular magnetic anisotropy in half-metallic magnetic Heusler epitaxial thin films. *Phys. Rev. Appl.* **2023**, *20*, 054017. [CrossRef]
21. Lou, K.; Xie, T.; Zhao, Q.; Jiang, B.; Xia, C.; Zhang, H.; Yao, Z.; Bi, C. Perpendicular magnetic anisotropy in as-deposited CoFeB/MgO thin films. *Appl. Phys. Lett.* **2022**, *121*, 122401. [CrossRef]
22. Devolder, T.; Couet, S.; Swerts, J.; Liu, E.; Lin, T.; Mertens, S.; Kar, G.; Furnemont, A. Annealing stability of magnetic tunnel junctions based on dual MgO free layers and [Co/Ni] based thin synthetic antiferromagnet fixed system. *J. Appl. Phys.* **2017**, *121*, 113904. [CrossRef]
23. Law, W.C.; Jin, T.L.; Zhu, X.T.; Nistala, R.R.; Thiyagarajah, N.; Seet, C.S.; Lew, W.S. Perpendicular magnetic anisotropy in Co/Pt multilayers induced by hcp-Ho at 400 °C. *J. Magn. Magn. Mater.* **2019**, *477*, 124–130. [CrossRef]
24. Garzón, E.; De Rose, R.; Crupi, F.; Trojman, L.; Teman, A.; Lanuzza, M. Adjusting thermal stability in double-barrier MTJ for energy improvement in cryogenic STT-MRAMs. *Solid-State Electron.* **2022**, *194*, 108315. [CrossRef]
25. Sun, Y.; Meng, F.; Gong, J.; Gao, Y.; Chen, R.; Zhao, L.; Zeng, D.; Fu, T.; He, W.; Wang, Y. Optimization of bifurcated switching by enhanced synthetic antiferromagnetic layer. *Electronics* **2024**, *13*, 4771. [CrossRef]
26. Verbeno, C.H.; Zázvorka, J.; Nowak, L.; Veis, M. Magnetic coercivity control via buffer layer roughness in Pt/Co multilayers. *J. Magn. Magn. Mater.* **2023**, *585*, 171124. [CrossRef]
27. Huang, D.; Zhang, D.; Kim, Y.; Wang, J.-P.; Wang, X. Magnetization dynamics in synthetic antiferromagnets with perpendicular magnetic anisotropy. *Phys. Rev. B* **2023**, *107*, 214438. [CrossRef]
28. Parkin, S.S.P.; Bhadra, R.; Roche, K.P. Oscillatory magnetic exchange coupling through thin copper layers. *Phys. Rev. Lett.* **1991**, *66*, 2152. [CrossRef]
29. Chatterjee, J.; Auffret, S.; Sousa, R.; Coelho, P.; Prejbeanu, I.L.; Dieny, B. Novel multifunctional RKKY coupling layer for ultrathin perpendicular synthetic antiferromagnet. *Nat. Sci. Rep.* **2018**, *8*, 11724. [CrossRef]
30. Parkin, S.S.P. Systematic variation of the strength and oscillation period of indirect magnetic exchange coupling through the *3d*, *4d*, and *5d* transition metals. *Phys. Rev. Lett.* **1991**, *67*, 3598. [CrossRef]
31. Stiles, M.D. Interlayer exchange coupling. *J. Magn. Magn. Mater.* **1999**, *200*, 322–337. [CrossRef]
32. Bloemen, P.J.H.; van Kesteren, H.W.; Swagten, H.J.M.; de Jonge, W.J.M. Oscillatory interlayer exchange coupling in Co/Ru multilayers and bilayers. *Phys. Rev. B* **1994**, *50*, 13505. [CrossRef]
33. Karayev, S.; Murray, P.D.; Khadka, D.; Thapaliya, T.R.; Liu, K.; Huang, S.X. Interlayer exchange coupling in Pt/Co/Ru and Pt/Co/Ir superlattices. *Phys. Rev. Mater.* **2019**, *3*, 041401. [CrossRef]
34. Zhang, D.L.; Sun, C.; Lv, Y.; Schliep, K.B.; Zhao, Z.; Chen, J.Y.; Voyles, P.M.; Wang, J.P. L 10 Fe−Pd Synthetic Antiferromagnet through an fcc Ru spacer utilized for perpendicular magnetic tunnel junctions. *Phys. Rev. Appl.* **2018**, *9*, 044028. [CrossRef]
35. Haoran Xu, H.; Chen, F.; Chen, B.; Jin, F.; Ma, C.; Xu, L.; Guo, Z.; Qu, L.; Lan, D.; Wu, W. Synthetic Antiferromagnets with Steplike Hysteresis Loops and High-T_C Based on All-Perovskite $La_{0.7}Sr_{0.3}MnO_3$ Superlattices. *Phys. Rev. Appl.* **2018**, *10*, 024035.
36. Almasi, H.; Sun, C.L.; Li, X.; Newhouse-Illige, T.; Bi, C.; Price, K.C.; Nahar, S.; Grezes, C.; Hu, Q.; Khalili Amiri, P.; et al. Perpendicular magnetic tunnel junction with W seed and capping layers. *J. Appl. Phys.* **2017**, *121*, 153902. [CrossRef]
37. Kim, G.; Lee, S.; Lee, S.; Song, B.; Lee, B.K.; Lee, D.; Lee, J.S.; Lee, M.H.; Kim, Y.K.; Park, B.G. The influence of capping layers on tunneling magnetoresistance and microstructure in CoFeB/MgO/CoFeB magnetic tunnel junctions upon annealing. *Nanomaterials* **2023**, *13*, 2591. [CrossRef]
38. Frankowski, M.; Żywczak, A.; Czapkiewicz, M.; Ziętek, S.; Kanak, J.; Banasik, M.; Powroźnik, W.; Skowroński, W.; Chęciński, J.; Wrona, J.; et al. Buffer influence on magnetic dead layer, critical current, and thermal stability in magnetic tunnel junctions with perpendicular magnetic anisotropy. *J. Appl. Phys.* **2015**, *117*, 223908. [CrossRef]
39. Ghemes, C.; Tibu, M.; Dragos-Pinzaru, O.-G.; Ababei, G.; Stoian, G.; Lupu, N.; Chiriac, H. Optimization of magnetic tunnel junction structure through component analysis and deposition parameters adjustment. *Materials* **2024**, *17*, 2554. [CrossRef]

40. Liu, E.; Swerts, J.; Devolder, T.; Couet, S.; Mertens, S.; Lin, T.; Spampinato, V.; Franquet, A.; Conard, T.; van Elshocht, S.; et al. Seed layer impact on structural and magnetic properties of [Co/Ni] multilayers with perpendicular magnetic anisotropy. *J. Appl. Phys.* **2017**, *121*, 043905. [CrossRef]
41. Won, Y.C.; Lim, S.H. Interfacial properties of [Pt/Co/Pt] trilayers probed through magnetometry. *Sci. Rep.* **2021**, *11*, 10779. [CrossRef]
42. Ma, M.; Wu, J.; Liu, B.; Wang, L.; Li, Z.; Ruan, X.; Hu, Z.; Wang, F.; Lu, X.; Liu, T.; et al. Optical Control of RKKY Coupling and Perpendicular Magnetic Anisotropy in A Synthetic Antiferromagnet. *Nat. Commun.* **2025**, *16*, 4401. [CrossRef] [PubMed]
43. Cuchet, L.; Rodmacq, B.; Auffret, S.; Sousa, R.C.; Prejbeanu, I.L.; Dieny, B. Perpendicular Magnetic Tunnel Junctions with A Synthetic Storage or Reference Layer: A New Route towards Pt- and Pd-Free Junctions. *Sci. Rep.* **2016**, *6*, 21246. [CrossRef]
44. Cho, J.; Kim, J.-S. Introduction of RKKY-pMTJ-Based Ultrafast Magnetic Sensor Architecture and Magnetic Multilayer Optimization. *Sensors* **2025**, *25*, 6793. [CrossRef]
45. Liu, X.; Mazumdar, D.; Shen, W.; Schrag, B.D.; Xiao, G. Thermal Stability of Magnetic Tunneling Junctions with MgO barriers for High Temperature Spintronics. *Appl. Phys. Lett.* **2006**, *89*, 023504. [CrossRef]
46. Schnitzspan, L.; Cramer, J.; Kubik, J.; Tarequzzaman, M.; Jakob, G.; Klaui, M. Impact of Annealing Temperature on Tunneling Magnetoresistance Multilayer Stacks. *IEEE Magn. Lett.* **2020**, *11*, 4503705. [CrossRef]
47. Parlak, U.; Aköz, M.E.; Tokdemir Öztürk, S.; Erkovan, M. Thickness Dependent Magnetic Properties of Polycrystalline Nickel Thin Films. *Acta Phys. Pol. A* **2015**, *127*, 995–997. [CrossRef]
48. Parlak UAköz, M.E.; Erkovan, M. Coexistence of Perpendicular and Parallel Exchange Bias Effects on Ni/CoO Bilayer. *J. Supercond. Nov. Magn.* **2016**, *29*, 1851–1854. [CrossRef]
49. Erkovan, M.; Aköz, M.E.; Parlak, U.; Öztürk, O. The Study of Exchange Bias Effect in Pt_xCo_{1-x}/CoO Bilayers. *J. Supercond. Nov. Magn.* **2017**, *30*, 2909–2913. [CrossRef]
50. Alpaslan Kösemen, Z.; Kösemen, A.; Öztürk, S.; Canımkurbey, B.; Erkovan, M.; Yerli, Y. Performance improvement in photosensitive organic field effect transistor by using multi-layer structure. *Thin Solid Film.* **2019**, *672*, 90–99. [CrossRef]
51. Kang, B.; Hwang, Y.H.; Kim, Y.J.; Lee, J.S.; Song, S.H.; Lee, S.; Lee, J.; Lee, O.; Park, S.Y.; Ju, B.K. Effects of buffer and capping layers on thermal stability of CoFeB/MgO frames at various temperatures. *Appl. Sci.* **2024**, *14*, 2394. [CrossRef]
52. Czapkiewicz, M.; Kanak, J.; Stobiecki, T.; Kachiel, M.; Zoladz, M.; Sveklo, I.; Maziewski, A.; van Dijken, S. Micromagnetic Properties of Co/Pt Multilayers Deposited on Various Buffer Layers. *Mater. Sci.-Pol.* **2008**, *26*, 839–849.
53. Emori, S.; Beach, G.S.D. Optimization of Out-of-Plane Magnetized Co/Pt Multilayers with Resistive Buffer Layers. *J. Appl. Phys.* **2011**, *110*, 033919. [CrossRef]
54. Yang, C.L.; Lai, C.H. High thermal durability of Ru-based synthetic antiferromagnet by interfacial engineering with Re insertion. *Nat. Sci. Rep.* **2021**, *11*, 15214. [CrossRef] [PubMed]
55. Lim, S.T.; Tran, M.; Chenchen, J.W.; Ying, J.F.; Han, G. Effect of different seed layers with varying Co and Pt thicknesses on the magnetic properties of Co/Pt multilayers. *J. Appl. Phys.* **2015**, *117*, 17A731. [CrossRef]

Disclaimer/Publisher's Note: The statements, opinions and data contained in all publications are solely those of the individual author(s) and contributor(s) and not of MDPI and/or the editor(s). MDPI and/or the editor(s) disclaim responsibility for any injury to people or property resulting from any ideas, methods, instructions or products referred to in the content.